NKCC1 cotransporter inactivation underlies embryonic development of chloride-mediated inhibition in mouse spinal motoneuron

Alain Delpy, Anne-Emilie Allain, Pierre Meyrand and Pascal Branchereau

Centre de Neuroscience Intégratives et Cognitives, Université Bordeaux and CNRS, UMR 5228, Avenue des Facultés, 33405 Talence cedex, France

Early in development, GABA and glycine exert excitatory action that turns to inhibition due to modification of the chloride equilibrium potential (E_{Cl}) controlled by the KCC2 and NKCC1 transporters. This switch is thought to be due to a late expression of KCC2 associated with a NKCC1 down-regulation. Here, we show in mouse embryonic spinal cord that both KCC2 and NKCC1 are expressed and functional early in development (E11.5–E13.5) when $GABA_A$ receptor activation induces strong excitatory action. After E15.5, a switch occurs rendering GABA unable to provide excitation. At these subsequent stages, NKCC1 becomes both inactive and less abundant in motoneurons while KCC2 remains functional and hyperpolarizes E_{Cl}. In conclusion, in contrast to other systems, the cotransporters are concomitantly expressed early in the development of the mouse spinal cord. Moreover, whereas NKCC1 follows a classical functional extinction, KCC2 is highly expressed throughout both early and late embryonic life.

(Received 8 October 2007; accepted after revision 13 December 2007; first published online 20 December 2007)
Corresponding author P. Branchereau: Centre de Neuroscience Intégratives et Cognitives, Université Bordeaux et Centre National de la Recherche Scientifique Unité Mixte de Recherche 5228, Avenue des Facultés, 33405 Talence, France. Email: p.branchereau@cnic.u-bordeaux1.fr

In the mature central nervous system (CNS), the two main inhibitory neurotransmitters are GABA and glycine. They activate ionotropic chloride-permeable channels when binding to $GABA_A$ and glycine receptors $GABA_AR$, and GlyR respectively. Therefore $GABA_AR$- and GlyR-dependent effects are mainly dependent upon the chloride equilibrium potential (E_{Cl}). In mature neurons, because the intracellular Cl^- concentration $[Cl^-]_i$ is drastically lowered, the activation of chloride-permeable channels by GABA or glycine induces a chloride influx. However, in immature neurons, due to a higher $[Cl^-]_i$, GABA and glycine act as excitatory neurotransmitters (e.g. Owens & Kriegstein, 2002). During the maturation of the CNS, a switch from excitatory to inhibitory effects of GABA/glycine occurs at different developmental stages depending on the brain structures. In the pyramidal hippocampal neurons, the switch takes place after post-natal day 10 (P10) (Ben-Ari *et al.* 1989; Khazipov *et al.* 2004; Banke & McBain, 2006) whereas it happens before P9 in the lateral superior olive (LSO) (Ehrlich *et al.* 1999; Balakrishnan *et al.* 2003), in the pre-Botzinger complex (Ritter & Zhang, 2000) and in the hypoglossal motoneurons (Singer *et al.* 1998). In spinal superficial dorsal horn neurons, the anion gradient shift is completed by P7 (Baccei & Fitzgerald, 2004; Cordero-Erausquin *et al.* 2005). The lowering of intracellular chloride concentration during the course of the development has been extensively studied and relies on the differential ontogenic expression of the Na^+–K^+–$2Cl^-$ cotransporter isoform 1 (NKCC1), which takes up chloride ions (Alvarez-Leefmans *et al.* 1988; Rohrbough & Spitzer, 1996; Russell, 2000), and the neuronal K^+–Cl^- cotransporter type 2 (KCC2) (Payne *et al.* 1996), which extrudes chloride ions (Rivera *et al.* 1999; Hubner *et al.* 2001). It is generally accepted that, early in development, NKCC1 is predominant and therefore maintains a high $[Cl^-]_i$ while later NKCC1 vanishes and KCC2 develops, lowering intracellular chloride levels (Ben-Ari, 2001, 2002; Owens & Kriegstein, 2002).

Although the organization of spinal locomotor networks is extensively studied (Vinay *et al.* 2000; Kiehn & Butt, 2003; Clarac *et al.* 2004; Kiehn, 2006), the development of GABA/glycine inhibitions within these networks still remains elusive. The general consensus is that bilateral alternating motor outputs are coordinated by reciprocal inhibitory interactions between rhythm-generating networks located on both sides of the spinal cord (Grillner & Wallen, 1985). First alternations between antagonistic pools of lumbar motoneurons are observed at late embryonic stages (E17.5 in the mouse, E20.5 in the rat), suggesting that functional

A. Delpy and A.-E. Allain contributed equally to this work.

 DOI: 10.1113/jphysiol.2007.146993

inhibition is already present at embryonic stages (Kudo & Nishimaru, 1998; Branchereau *et al.* 2000). However, available data on the involvement of GABA/glycine transmission in locomotor rhythms mainly concern postnatal stages (Hinckley *et al.* 2005; Jean-Xavier *et al.* 2006; Quinlan & Kiehn, 2007) and fetal development of the chloride-dependent switch from excitation to inhibition has never been studied in detail in motoneurons. Some studies have been performed on GABA/glycine development but these studies have focused on the analysis of spontaneous transmission (Gao *et al.* 1998, 2001) or glycine- and GABA-induced effects in current-clamp mode (Wu *et al.* 1992).

We have previously shown that the GABA and glycine phenotypes emerge at early embryonic stages (E12.5–E13.5 at lumbar level) (Allain *et al.* 2004, 2006), and that a switch from excitatory to inhibitory actions of GABA/glycine probably develops after E14.5 (Branchereau *et al.* 2002). However, these conclusions are drawn from extracellular ventral root recordings and thus are indirect. In the present study, therefore, we investigated, in lumbar motoneurons, whether a switch from excitatory to inhibitory effects of GABA/glycine occurs during mouse embryonic life. The respective role of KCC2 and NKCC1 in these changes was assessed. We show that GABA effects remain depolarizing and that spike threshold is constant throughout ontogeny. However, after E15.5, E_{Cl} sharply drops. As a consequence, after this stage, the depolarizing effect due to $GABA_AR$ activation fails to trigger action potentials. Using immunohistochemistry, we demonstrate that KCC2 and NKCC1 are present as early as E11.5 in the lumbar area and remain detectable until birth. Our combined electrophysiological and pharmacological results indicate that whereas early in development both cotransporters are functional, NKCC1 inactivates after E15.5 and only KCC2 remains functional. Preliminary results have been presented in abstract form (Delpy *et al.* 2006).

Methods

Animals and isolation of spinal cords

Pregnant adult and newborn OF1 mice (Charles River Laboratories, France) were maintained and killed according to protocols approved by the European Community Council and conforming to NIH *Guidelines for Care and Use of Laboratory Animals*. Embryonic day 0.5 (E0.5) corresponded to the day following the mating night, i.e. day 0.5 of gestation (confirmed by the observation of a vagina plug in Charles River Laboratories), and postnatal day 0 (P0 = E19.5) corresponded to the date of birth. Experiments were carried out on embryos at E11.5, E12.5, E13.5, E14.5, E15.5, E16.5, E17.5, E18.5 and on newborn mice at P0. Embryos were surgically removed from pregnant mice killed by cervical dislocation. Newborn mice were decapitated. For immunohistochemical study, embryos and newborns were rinsed with Dulbecco's phosphate-buffered saline (PBS) at 6–8°C, and their spinal cords with dorsal root ganglia dissected. For electrophysiology, brainstem–spinal cord was dissected, dorsally opened (Fig. 1*A*1) and the meninges removed. The neuraxis in 'open-book' configuration (Fig. 1*A*2) was continuously perfused at 30 ± 2°C (perfusion rate of 3–5 ml min^{-1}; chamber volume of 1.5 ml) with physiological solution that contained the following (mM): 113 NaCl, 25 $NaHCO_3$, 11 D-glucose, 4.5 KCl, 2 $CaCl_2$, 1 $MgCl_2$ and 1 NaH_2PO_4 (equilibrated with 95% O_2–5% CO_2).

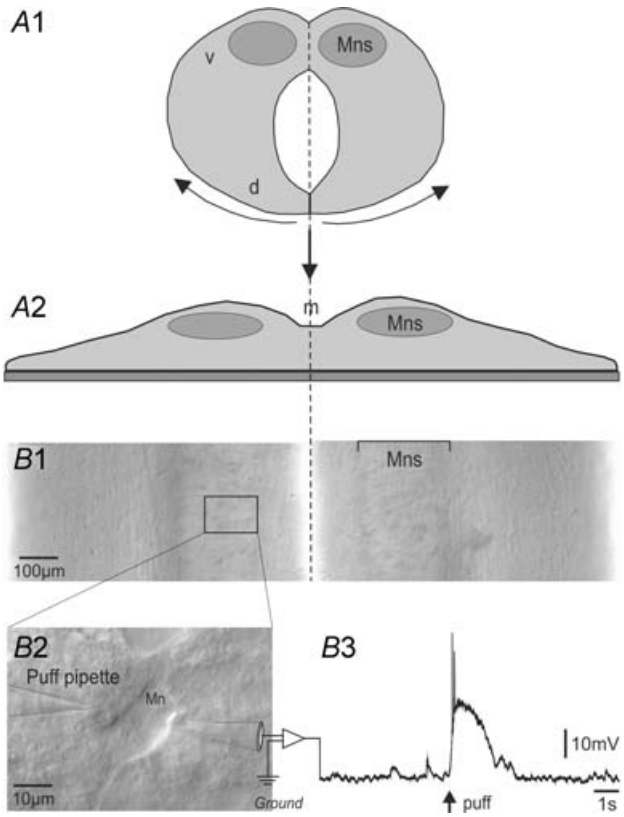

Figure 1. Schematic representation of the *in vitro* embryonic mouse spinal cord preparation used for electrophysiology
A, dissection procedure. After removing the meninges, the spinal cord is dorsally opened (*A*1) and positioned in the recording chamber ventral side up allowing direct access to motoneurons. *A*2, schematic view of coronal section of the opened spinal cord. *B,* patch-clamp recording of visually identified motoneurons. Partial upper view of the laid down spinal cord (*B*1). The dashed line indicates the midline (m) with the two symmetric columns of motoneurons, laterally positioned. *B*2, example of a visually identified motoneuron showing the relative position of puff pipette used to eject pharmacological agents and the patch-clamp pipette. *B*3, perforated patch clamp recording of a motoneuron. The depolarization is due to pressure ejection of the $GABA_AR$ agonist isoguvacine. d, dorsal zone; m, midline; Mns, motoneuronal column; v, ventral zone.

Immunofluorescence

Immunostaining was processed either on spinal cord transverse sections or on entire spinal cords after their use in electrophysiology. Spinal cords were fixed in 2% paraformaldehyde for 2–3 h at room temperature. They were then rinsed with 0.1 M PBS. For the immunohistochemical procedure on transverse spinal cord sections, the lumbar part (L1–L5) was isolated and cryoprotected at 4°C in sucrose (15% and then 30%) made in 0.1 M phosphate buffered (pH 7.4). The tissue was embedded in a plastic resin (Tissue-Tek, Sakura Finetek Europe B.V., Zoeterwoude, the Netherlands) and quickly frozen by using isopentane cooled with liquid nitrogen. Then, 25 μm-thick serial sections were transversally cut using a cryostat (Kryostat 1720, Leitz, Wetzlar, Germany).

Entire fixed spinal cords containing Neurobiotin-injected motoneurons or transverse lumbar sections were incubated in primary antibody for 48 h at 4°C in 0.1 M PBS containing 0.2% bovine serum albumin (BSA, Sigma, St Louis, MO, USA) and 0.1% Triton X-100 (Sigma). Primary antibodies used in the present study were the following: rabbit polyclonal anti-KCC2 (1/400) (from Upstate Lake Placid, NY, USA; distributed by Millipore S.A.S., Saint-Quentin-en-Yvelines, France), rabbit polyclonal anti-rat NKCC1 (1/200, US Biological, distributed by Euromedex, Souffelweyersheim, France), mouse monoclonal anti-NKCC1 T4 (1/200, Developmental Studies Hybridoma Bank, The University of Iowa, IA, USA) and mouse monoclonal anti-Islet1/2 (1/100, Developmental Studies Hybridoma Bank). In order to reveal Neurobiotin-injected neurons, streptavidin-Cy3 (1/400, Invitrogen SARL, Cergy Pontoise, France) was added to the primary antibody solution. After rinsing, spinal cords were incubated at room temperature for 2 h in the appropriate following secondary antibodies (from Invitrogen SARL): Alexa-Fluor 488 $F(ab')_2$ fragment of goat anti-rabbit IgG (H + L), Alexa-Fluor 488 $F(ab')_2$ fragment of goat anti-mouse IgG (H + L), Alexa-Fluor 546 goat anti-mouse IgG (H + L) or Alexa-Fluor 647 goat anti-mouse IgG (H + L) 1/400. After three rinses (at least 10 min each), the preparations were mounted in a mixture containing 90% glycerol and 10% PBS to which was added 2.5% 1,4-diazabicyclo[2,2,2]octane (DABCO, Sigma) to reduce the rate of fluorescence quenching. For the immunohistological study, 70 embryos (9 E11.5, 12 E12.5, 10 E13.5, 12 E14.5, 9 E15.5, 13 E16.5, 5 E17.5) and 12 P0 pups were used. Control immunohistological experiments were performed without the primary or secondary antibody. No labelling was obtained under these conditions.

Confocal microscopy

Preparations were viewed with a BX51 Olympus Fluoview 500 confocal microscope equipped with blue argon (488 nm), green helium–neon (543 nm) and red helium–neon (633 nm) laser sources. For quantitative analysis of NKCC1 and KCC2 immunoreactivity on spinal cord transverse sections, 0.8 and 0.3 μm serial optical sections were imaged either with a ×10 objective or a ×40 oil objective. For triple labelling of KCC2 and NKCC1 and visualization of injected neurons in entire spinal cords, 0.2 μm serial optical sections (1024 pixels × 1024 pixels) were imaged with a ×60 oil-immersion objective with a numerical aperture of 0.90. Average images were then acquired by sequential scanning for FITC, Cy3 and Cy5 detection. Unless otherwise stated, images presented in this study are stacked projections of 2–4 optical sections.

Image analysis, quantification and statistics

The ventro-dorsal distribution of KCC2 and NKCC1 immunoreactivity was analysed from transverse sections of the lumbar spinal cord. For the macroscopic analysis of the intensity of labelling in the ventral area, we used ImageJ 1.37v (Wayne Rasband, National Institutes of Health, USA) to analyse confocal projection images from 10 optical planes (0.8 μm thick) acquired using the ×10 objective. Data are presented in histograms in which each bar corresponds to the average of 4–12 values, from at least 2–3 embryos (2–3 different litters). Each value corresponds to the mean intensity of immunofluorescence calculated by ImageJ on selected ventral areas (see white circles in Fig. 2). For each value, the background fluorescence signal is subtracted from signal from selected areas. Limits of these zones were arbitrarily chosen as delineating the vicinity of the motoneuronal pools. Therefore, these zones were larger for late developmental stages (compare circles in Fig. 2*A*1 and 4). All measurements correspond to the mean fluorescence density. For the microscopic analysis of the intensity of NKCC1 and KCC2 labelling in the cytoplasm or in the vicinity of the plasma membrane, Neurobiotin-filled motoneurons were processed for triple immunolabelling. Clusters of NKCC1 and KCC2 labelling were counted manually in two optical sections randomly chosen at the level of the soma of Neurobiotin-injected motoneurons. A cluster was characterized by a sharp increase of fluorescence intensity. Clusters located less than 4 pixels from the outline of the Neurobiotin-injected motoneuron were considered as in the vicinity of the plasma membrane. Other clusters were considered to be in the cytoplasm. Data were collected from 5–6 injected motoneurons coming from different embryos (3 different litters) and were expressed as density (number of clusters per volume of motoneuron somata, in μm^3). All values were expressed as mean ± standard error of the mean (S.E.M.). Statistical significance of the difference was assessed either by a one-way ANOVA followed by pairwise multiple *post hoc* comparisons (Tukey's test) or by a non-parametric unpaired *t* test (GraphPad Software, San Diego, CA, USA). The level of significance was set at $P < 0.05$.

Perforated patch clamp recordings

We performed perforated-patch recordings on motoneurons. These latter were identified according to their morphological features (pear-shaped large cell body) and their disposition in columns in the ventral horn (Fig. 1*B*1 and 2). To confirm that these criteria were sufficient to identify motoneurons, we performed, at different stages, Islet1/2-Neurobiotin double staining (data not shown).

An Olympus BX51WI microscope equipped with differential interference contrast (DIC) and a CCD camera (SPOT RT-SE6, Diagnostic Instruments, Sterling Heights, MI, USA) was used to visualize motoneurons. Patch electrodes were constructed from thin-walled single-filamented borosilicate glass (1.5 mm outer diameter; Harvard Apparatus, Les Ulis, France) using a two-stage vertical microelectrode puller (PP-830; Narishige, Tokyo, Japan). Pipette resistances ranged from 3 to 5 MΩ, and only seal resistances > 10 GΩ were kept. Patch electrodes were positioned on visually identified motoneurons using motorized micromanipulators (Luigs & Neumann, Ratingen, Germany). For perforated patch clamp experiments, gramicidin (Sigma) stock solution was dissolved at 1–2 mg ml^{-1} in DMSO (Sigma). Electrode tips were filled with a filtered patch solution containing the following (mM): 130 KCl, 10 Hepes, 10 EGTA, and 2 MgATP, pH 7.4 (284 mosmol l^{-1}) and subsequently backfilled with gramicidin diluted in the same solution to a final concentration of 10–20 μg ml^{-1}. Access resistance (R_a) was monitored rigorously throughout experiments and over the course of 70–90 min stabilized at 40 ± 5 MΩ ($n = 120$). Recordings did not commence until the R_a had stabilized. R_a compensation was not applied. For intracellular injections, we performed whole-cell recordings using pipettes containing Neurobiotin (0.4%) (CliniSciences, Montrouge, France) diluted in the following medium (mM): 130 potassium gluconate, 10 Hepes, 10 EGTA, 5 NaCl, 2 MgATP and 1 $CaCl_2$, pH 7.4 (296 mosmol l^{-1}). All recordings were made with an Axon Multiclamp 700B amplifier (Molecular Devices, Sunnyvale, CA, USA), data were low-pass filtered (2.4 kHz) and acquired at 10 kHz on a computer using an analog-to-digital converter (Digidata 1322A; Molecular Devices), and a data acquisition software (Clampex 9.2; Molecular Devices). Measurements were corrected for liquid junction potentials (3.4 mV, calculated using the Clampex junction potential calculator). Using the Nernst equation, E_{Cl} between intra and extrapipette solution was calculated to be +1.5 mV. Thus, to confirm that the perforated-patch configuration had not ruptured during the experiment, repetitive E_{Cl} tests were performed. Measurements leading to an E_{Cl} close to 0 mV were considered as whole-cell recordings and cells were then discarded. The Clampex membrane test was used to monitor the input resistance (R_{in}) and membrane capacitance: a −60 mV holding membrane potential and 5 mV steps (negative and positive, 40 ms duration) were chosen. Reversal potential for chloride ions (E_{Cl} or EGABA$_A$R) was calculated by a linear fit (GraphPad Software).

High input resistances of immature motoneurons may lead to erroneous values of resting membrane potential (V_{rest}), spike threshold and E_{Cl}. The error comes from a leak between the patch pipette and the sealed membrane. A model and equation was proposed to compensate the inaccuracy (Tyzio *et al.* 2003). The equation is given by

$$E'_m = E^0_m \times \frac{R_{ps} - R_{in}}{R_{ps}} + E_{ps}\frac{R_{in}}{R_{ps}} \Rightarrow$$

$$E^0_m = \left(E'_m - E_{ps} \times \frac{R_{in}}{R_{ps}}\right) \times \frac{R_{ps}}{R_{ps} - R_{in}}$$

where E'_m is the measured value, E^0_m is the compensated value, R_{ps} is the seal resistance (always > 10 GΩ), R_{in} is the input resistance of the recorded motoneuron and E_{ps} is the liquid junction potential between bath and intrapipette solutions (3.4 mV). As demonstrated in Tyzio's study, this equation is valid when the ratio between the input resistance (R_{in}) and the seal resistance (R_{ps}) is < 0.4. Because this is always the case in our measurements ($R_{in}/R_{ps} \leq 0.1$), we used the proposed equation to compensate this error. All data are then corrected values.

Pharmacological agents

Patch-clamp pipettes were used to pressure-apply the GABA$_A$R agonist isoguvacine. The drug ejection (4 p.s.i., 20–30 ms duration) was performed with a PicoSpritzer III (Parker Hannifin Corporation, Fairfield, NJ, USA). Isoguvacine (100 μM, Tocris Bioscience, Bristol, UK) was dissolved in the physiological solution. The two following drugs were bath applied: the NKCC1 blocker bumetanide (Sigma, 10–20 μM) that was perfused for 40 min, and the KCC2 blocker furosemide (frusemide) (Sigma, 50–200 μM), applied for 5 min. Drugs were first dissolved in DMSO and then diluted in the physiological solution to their final concentration.

Results

Ontogeny of KCC2 and NKCC1 immunoreactivity

The use of immunohistochemical methods allowed us to follow the development of the two cotransporters KCC2 and NKCC1 proteins on lumbar transverse sections of embryonic spinal cords. Our data indicate that as early as E11.5, KCC2-immunoreactivity (KCC2-ir) was detected in

the ventral part of the spinal cord, specifically in the future grey matter (Fig. 2*A*1). Moreover, using double staining with the motoneuronal-specific antibody Islet1/2 and antibody KCC2 we found that this labelling included all motoneuronal pools (data not shown). No KCC2 staining could be detected in the marginal zone and in dorsal parts of the spinal cord (Fig. 2*A*1). After E11.5, from the ventral area, the KCC2-ir expanded dorsally (Fig. 2*A*2–6). At E12.5, the whole ventral area was enriched with KCC2-ir and the medio-lateral part of the dorsal area started to be stained. Again, the marginal zone was devoid of KCC2-ir (mz, Fig. 2*A*2). One day later, the staining invaded the

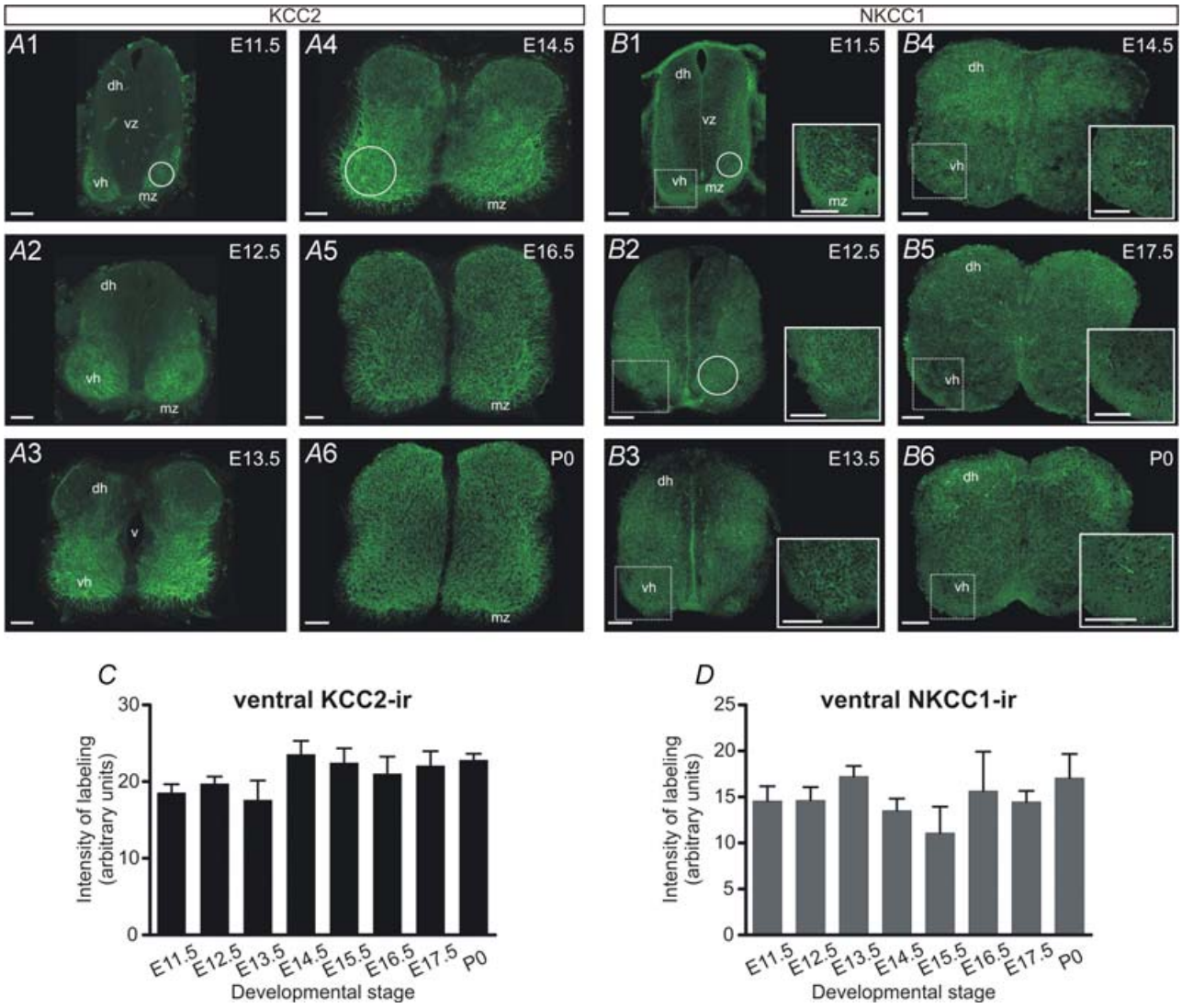

Figure 2. Embryonic maturation of KCC2 and NKCC1 at lumbar level
*A*1, KCC2-ir on a frontal section of lumbar spinal cord at E11.5. Note that the staining is restricted to the ventro-lateral grey matter in the ventral area (v). *A*2, at E12.5, KCC2-ir has expanded to the whole ventral grey matter. *A*3, at E13.5, the KCC2-ir is detected in the dorsal zone and in dorso-medial areas. *A*4, at E14.5, the whole grey matter shows KCC2-ir with a stronger staining in ventral areas compared to dorsal. *A*5 and 6, from E16.5 to P0, KCC2-ir spreads across the entire grey matter. *B*1, at E11.5, NKCC1-ir is detected in the ventro-lateral and dorso-lateral grey matter and in the marginal zone. The inset, in the bottom right-hand corner shows, as for all panels, a higher magnification of the NKCC1 staining within the motoneuronal area corresponding to boxed areas drawn on the global view. *B*2 and 3, from E12.5 to E13.5, the NKCC1 staining remains stable in the ventral area whereas immunoreactivity progressively invades the entire dorsal zone. *B*4–6, from E14.5 to P0, NKCC1-ir remains detectable in the ventral area but appears stronger in the dorsal area. Staining was performed with the monoclonal T4 antibody. Scale bar, 100 μm. dh, dorsal horn; mz, marginal zone; v, ventricle. vh, ventral horn; vz, ventricular zone. *C* and *D,* quantitative analyses of mean KCC2- (*C*) and NKCC1-ir (*D*) in the ventral horn (see circled areas in *A* and *B*). Note that the mean intensity of both KCC2 and NKCC1 staining remains stable in the lumbar ventral area during ontogeny (no statistical differences between stages, one-way ANOVA). Each histogram corresponds to 4–12 preparations. Values are mean ± S.E.M.

medial part of the dorsal zone (Fig. 2*A*3) and the entire dorsal area at the E14.5 stage of development (Fig. 2*A*4). The pattern of KCC2 expression remained stable after E14.5 (Fig. 2*A*5–6). Although, there was no dense KCC2 staining in the marginal zone, it must be noted that from E13.5 to birth, KCC2-ir hairy processes projected into this future white matter (mz). In parallel with the embryonic development of the KCC2-ir, the NKCC1-ir was examined during the same ontogenetic period. In order to confirm the specificity of our NKCC1 labelling, two antibodies were used: a mouse monoclonal T4 and a rabbit polyclonal antibody. For all developmental stages, the overall pattern of NKCC1-ir was similar with both antibodies and this similarity was confirmed at higher magnification (data not shown). At E11.5, a dense NKCC1 labelling was already detected throughout the future ventral grey matter of the spinal cord (Fig. 2*B*1). Unlike KCC2-ir, the marginal zone was NKCC1 immunoreactive (inset Fig. 2*B*1). At E12.5, whereas NKCC1 staining remained stable in the ventral area of the spinal cord, NKCC1-ir invaded the dorso-lateral grey matter (Fig. 2*B*2). By E13.5, the entire dorsal grey matter presented NKCC1-ir (Fig. 2*B*3). Then, the staining remained strong in the ventral area but appeared denser in the dorsal areas from E14.5 to P0 (Fig. 2*B*4–6). Higher magnifications from the ventral motoneuronal area revealed a uniform punctiform staining distributed all over the future grey and white matter (insets Fig. 2). On the whole, for both cotransporters, the labelling first occurred always on the ventral part of the spinal cord and, although staining with both antibodies later covered the entire section, the NKCC1-ir seemed to reach the dorsal region before the KCC2-ir. In addition, two striking differences in the distribution of these two transporters were observed: first, the marginal zone did not exhibit significant KCC2-ir but was largely NKCC1 immunoreactive; second, after E16.5, the dorsal area seemed to express more NKCC1 than the ventral area while KCC2-ir was always stronger in the ventral zone. To better understand the physiological consequence of the expression of both cotransporters within the motoneuronal areas, a quantitative analysis of the mean fluorescence signal was performed at lumbar level in the labelled ventral horn (see circled areas in Fig. 2). Interestingly, within this ventral area either KCC2 or NKCC1-ir were detected as early as E11.5 and the level of macroscopic protein detection was not statistically different during the course of development (Fig. 2*C* and *D*).

To reveal the functional consequences of the ontogeny of these two cotransporters, we studied the maturation of chloride-mediated inhibitions in embryonic motoneurons. Although, for this study a prerequisite was to know the basic biophysical properties of the motoneurons recorded at different stages of embryonic development.

Maturation of biophysical properties of fetal mouse motoneurons

Before analysing the ontogenic evolution of E_{Cl} from E13.5 to birth and to understand the functional consequence on the operation of motor networks, a required knowledge concerns the evolution of motoneuronal features during the course of embryonic development. Four main biophysical parameters have been studied. The resting membrane potential V_{rest} and spike threshold give us the excitatory or inhibitory nature of $GABA_AR$-related transmission when compared to E_{Cl}. The input resistance (R_{in}) and membrane capacitance (C_m) are indices of transfer function from external synaptic inputs onto motoneurons and membrane surface, respectively.

In current-clamp mode, spikes occurred spontaneously at all stages. Figure 3*A* illustrates three motoneuronal recordings taken at E13.5, E16.5 and P0. To determine spiking threshold, positive steps of current were injected into the motoneurons until a spike was elicited. Spike threshold for motoneurons, measured and corrected at all stages of development, appeared stable and no statistical difference was observed between stages (Fig. 3*B*, linear regression slope not significantly different from 0, $P = 0.0885$). The mean value for all spike thresholds was -40.8 ± 0.6 mV ($n = 65$). By contrast, the ontogenic evolution of resting membrane potential was altered. Indeed, V_{rest} became more hyperpolarized: -55.4 ± 1.3 mV ($n = 19$) at E13.5, -65.0 ± 1.8 mV ($n = 13$) at E16.5 and -70.2 ± 1.0 mV ($n = 18$) at P0 (Fig. 3*C*, Table 1). Moreover, after this stage, the membrane potential was in the same range as the one described in mice in the first 2 weeks after birth (Stein *et al.* 2004). R_{in} exhibited a large decrease starting at a high level (up to 0.945 ± 0.096 GΩ) at E13.5 and then falling dramatically to less than 200 MΩ at E16.5 (Fig. 3*D*, Table 1). It must be noted that E15.5–E16.5 stages of development correspond to an ontogenetic time window when mature values of input resistance are reached. Finally, C_m increased quite continuously during the course of embryonic development (Fig. 3*E*, Table 1), suggesting that motoneurons become gradually larger.

Maturation of chloride-mediated inhibition in motoneurons

In a previous study, we have indirectly shown that inhibition between functionally antagonistic motoneurons developed in lumbar motor networks between E14.5 and E17.5 (Branchereau *et al.* 2002). In order to understand, at the cellular level, when and how this inhibition takes place in motoneurons, we undertook perforated patch clamp recordings during the course of embryonic development using the cation-specific pore-forming peptide gramicidin.

Such patch-clamp configuration was used in order to preserve the endogenous $[Cl^-]_i$. We examined the chloride concentration gradient by following the reversal potential of $GABA_AR$-mediated currents evoked by brief applications of the $GABA_AR$ agonist isoguvacine. Since the membrane potential slightly dropped during development (see Fig. 3*B*), we tested, under current clamp, the effect of $GABA_AR$ activation at two membrane potentials: −50 mV (i.e. close to immature value) and −70 mV (i.e. near mature value), at all stages of development. The

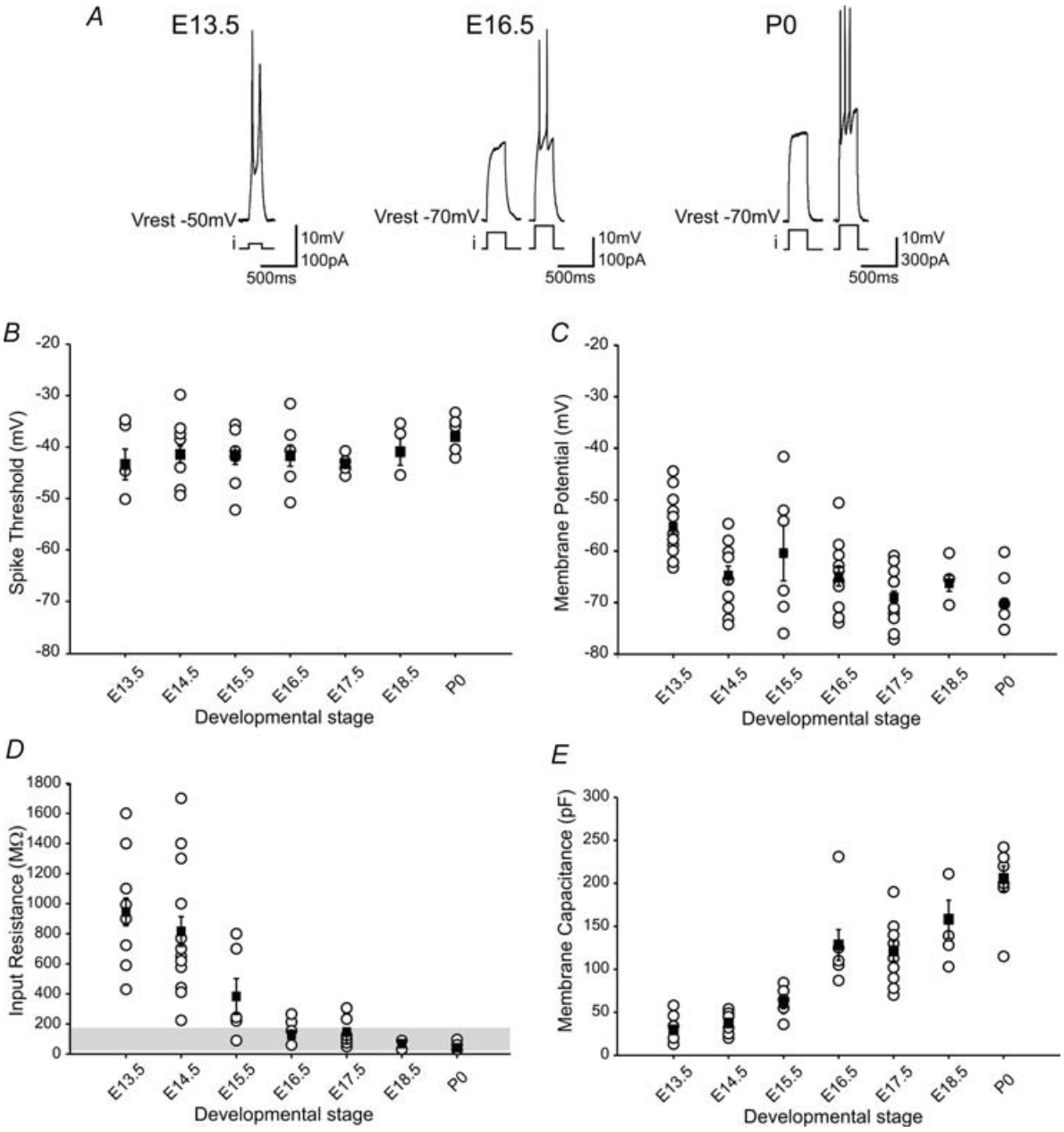

Figure 3. Ontogenic evolution of motoneuronal membrane properties from stages E13.5 to P0
A, comparison of motoneuronal response to depolarizing pulses, at E13.5, E16.5 and P0, showing that spike thresholds are similar at all stages of development whereas the resting membrane potential (V_{rest}) is 20 mV lower at E16.5 and P0 compared to E13.5. *B*, corrected spike threshold evolution throughout embryonic development. *C,* evolution of V_{rest} (corrected values) from E13.5 to P0. At each stage of development, circles represent individual measurement whereas black squares indicate mean values (± S.E.M.). *D*, evolution of motoneuronal R_{in}. The horizontal grey bar indicates the limits of the mature input resistance (between maximal and minimal S.E.M. values), between E16.5 and P0. *E,* maturation of motoneuronal membrane capacitance between E13.5 and P0. Values are given in Table 1.

Table 1. Ontogenic evolution of corrected resting membrane potential (V_{rest}) and spike threshold, membrane resistance (R_{in}) and capacitance (C_m) in lumbar spinal motoneurons (means ± S.E.M.)

Developmental stages:	E13.5	E14.5	E15.5	E16.5	E17.5	E18.5	P0
Spike threshold (mV)	−43.2 ± 2.7 ($n = 6$)	−41.3 ± 1.6 ($n = 13$)	−41.5 ± 1.8 ($n = 9$)	−41.6 ± 2.0 ($n = 8$)	−43.1 ± 0.7 ($n = 8$)	−40.8 ± 2.6 ($n = 4$)	−37.8 ± 0.8 ($n = 12$)
V_{rest} (mV)	−55.4 ± 1.3 ($n = 19$)	−64.8 ± 1.8 ($n = 6$)	−60.4 ± 5.4 ($n = 13$)	−65.0 ± 1.8 ($n = 16$)	−69.1 ± 1.2 ($n = 6$)	−66.3 ± 1.5 ($n = 18$)	−70.2 ± 1.0 ($n = 13$)
R_{in} (MΩ)	945 ± 96 ($n = 12$)	815 ± 98 ($n = 16$)	383 ± 130 ($n = 16$)	128 ± 34 ($n = 7$)	146 ± 23 ($n = 13$)	69.4 ± 11.1 ($n = 5$)	41.4 ± 11.4 ($n = 7$)
C_m (pF)	29.5 ± 3.6 ($n = 14$)	37.5 ± 2.6 ($n = 16$)	61.2 ± 7.7 ($n = 6$)	128.3 ± 19.4 ($n = 7$)	121.3 ± 12.1 ($n = 12$)	158.2 ± 24.8 ($n = 5$)	205.5 ± 15.1 ($n = 8$)

effects of isoguvacine are illustrated in Fig. 4 for three key stages: E13.5, E16.5 and P0. When the membrane potential was held at −50 mV, a depolarizing current pulse triggered an action potential whatever the stage of the embryonic development (Fig. 4*A*1–*C*1). However, whereas the $GABA_AR$ activation induced a depolarization at E13.5 (Fig. 4*A*1), such activation evoked a hyperpolarization at E16.5 and P0 (Fig. 4*B*1–*C*1), suggesting that, at these two stages, E_{Cl} was below −50 mV. When the membrane potential was maintained at −70 mV, a brief injection of depolarizing current induced again an action potential at the three stages (Fig. 4*A*2–*C*2). At E13.5, a brief application of isoguvacine triggered a large depolarization able to reach the spike threshold (Fig. 4*A*2). By contrast, at E16.5, although the $GABA_AR$ activation was still able to depolarize motoneurons, the observed depolarization did not generate an action potential (Fig. 4*B*2). At birth (P0), the isoguvacine application did not modify the membrane potential held at −70 mV (Fig. 4*C*2). These data suggest that the equilibrium potential for $GABA_AR$ shifts during the course of development toward negative values. To confirm this hypothesis, we performed voltage-clamp recordings from motoneurons at different stages of embryonic development (Fig. 5). At E13.5, when

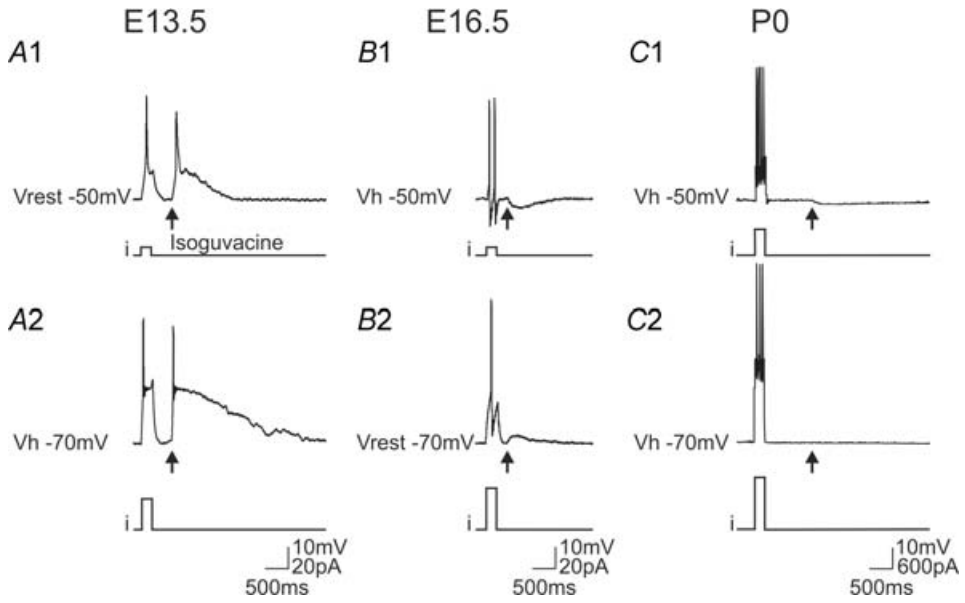

Figure 4. $GABA_AR$-induced effect on motoneuron membrane potential at E13.5, E16.5 and P0
A brief pulse of depolarizing current (i) is injected into recorded motoneurons in order to bring the membrane potential above spike threshold. Then, a brief pressure application of isoguvacine (100 μM, 20 ms, 4 p.s.i.) is used to activate $GABA_AR$. *A,* at E13.5, at resting membrane potential (V_{rest}, *A*1), either depolarizing current or application of isoguvacine elicits a depolarization, on top of which a spike is generated. The amplitude of this depolarization is increased when the membrane potential is held (V_h) at −70 mV and an action potential is still triggered. *B,* at E16.5, a depolarizing pulse of current still elicits an action potential whatever the membrane potential (*B*1, *B*2) whereas the stimulation of $GABA_AR$ evokes a hyperpolarization at V_h −50 mV (*B*1) and a depolarization at V_{rest} (*B*2). *C,* at birth the injected current triggers, at threshold level, a train of action potentials (*C*1, *C*2) whereas the application of isoguvacine still hyperpolarizes the membrane potential at V_h −50 mV (*C*1) but does not alter the membrane potential at V_h −70 mV (*C*2).

the holding potential was maintained at −50 mV, a brief application of the $GABA_AR$ agonist isoguvacine induced an inward current. The current was larger for more hyperpolarized holding potentials and reversed around −30 mV (Fig. 5*A*1). The plot of the $GABA_AR$-mediated current *versus* holding membrane potential (*I–V* plot) in this neuron indicated a reversal potential of −33 mV (Fig. 5*A*2). By contrast, in E16.5 motoneurons, at a holding membrane potential of −70 mV, a puff of isoguvacine triggered an inward current that reversed at −50 mV (Fig. 5*B*1 and 2). The same voltage-clamp protocol was carried out from E13.5 to P0 (Fig. 5*C*, black circles) and E_{Cl} values were compensated (see Methods). Although E_{Cl} shifted toward more hyperpolarized values day after day during the embryonic development, E_{Cl} decrease was not linear: the slow decline observed before E15.5 (ΔE_{Cl} from E13.5 to E15.5 was −4 mV) was followed by an abrupt reduction between E15.5 and E16.5 (ΔE_{Cl} from E15.5 to E16.5 was −14 mV). E_{Cl} did not express large fluctuations until E18.5. However, between E18.5 and birth, E_{Cl} kept falling (Fig. 5*C*). Table 2 stresses the evolution of E_{Cl} and intracellular chloride concentration $[Cl^-]_i$, calculated using the Nernst equation, during embryonic development.

To understand the functional consequence of the E_{Cl} level on motoneuronal excitability, we superimposed resting membrane potential and E_{Cl} on the same graph plots related to the ontogenetic evolution of spike threshold (Fig. 5*C*). Interestingly, until E15.5, the E_{Cl} was above the spike threshold whereas after E16.5, it dropped significantly below spike threshold ($P < 0.01$, unpaired *t* test for each stage). This graph also indicates that during the course of embryonic development, the resting membrane potential is always below the E_{Cl} value except at birth (P0) when E_{Cl} and resting membrane potential become not significantly different (unpaired *t* test) (-70.2 ± 2.7 mV, $n = 8$, for E_{Cl} and -70.2 ± 1.0 mV, $n = 18$, for resting membrane potential). Our data suggest that until E15.5, $GABA_AR$ activation may trigger action potentials whereas after E15.5 and until E18.5 such activation, although producing a depolarization, fails to trigger action potentials.

In conclusion, we show that, as demonstrated in other structures of the CNS, there is a shift of $GABA_AR$ equilibrium potential ($E_{GABA(A)R}$) toward negative values during the embryonic development of mouse lumbar spinal motoneurons. Such a shift was also observed for E_{GlyR} when glycine was applied to motoneurons in the same conditions (data not shown). It has been proposed that the maturation of the $GABA_AR$ equilibrium potential depends on variations in intracellular chloride concentration that are controlled by the two cotransporters KCC2 and NKCC1. Since our immunohistological study indicates that both KCC2 and NKCC1 are present between E11.5 and birth in the ventral motoneuronal area (see Fig. 2), we examined whether these cotransporters are always functional during ontogeny.

Functional implication of KCC2 and NKCC1 in the maturation of motoneuron inhibition

In order to identify at which developmental stages NKCC1 and KCC2 are active, we specifically blocked their action using pharmacological agents (bumetanide and furosemide, respectively), at three key developmental

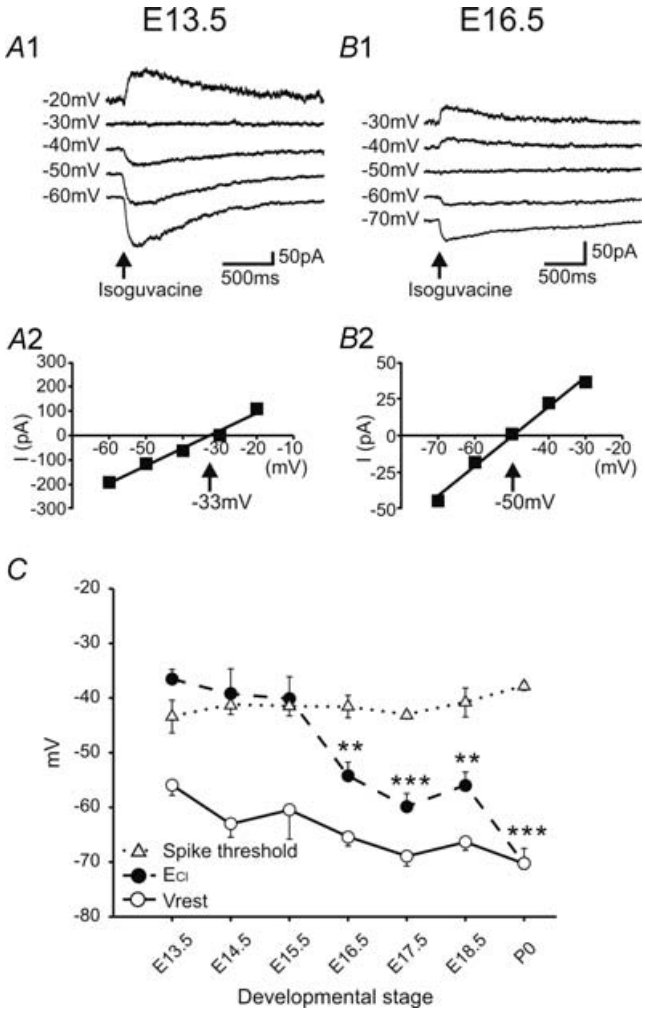

Figure 5. Embryonic maturation of $GABA_AR$-related effects on membrane potential
*A*1 and *B*1, perforated patch clamp recordings showing currents evoked by brief application of isoguvacine, from different holding potentials, at E13.5 (*A*1) and E16.5 (*B*1). Current *versus* voltage plots (same neurons shown in *A*1 and *B*1) allowing calculation of $GABA_AR$ equilibrium potential: −33 mV at E13.5 (*A*2) and −50 mV at E16.5 (*B*2) (measured by linear regression analysis, $r^2 > 0.96$ in both cases). *C,* evolution of corrected V_{rest} (white circles), spike threshold (grey triangles) and E_{Cl} (black circles) in motoneurons during embryonic development. From E13.5 to E15.5, spike threshold and E_{Cl} are not significantly different (non-parametric unpaired *t* test), whereas from E16.5 to birth, E_{Cl} is significantly lower than spike threshold (** $P < 0.01$; *** $P < 0.0001$). Values are means ± S.E.M. (*n* values indicated in Table 2).

Table 2. Maturation of E_{Cl} and $[Cl^-]_i$ in motoneurons (means ± S.E.M.)

Developmental stages:	E13.5	E14.5	E15.5	E16.5	E17.5	E18.5	P0
E_{Cl} (mV)	-36.7 ± 1.7 ($n = 18$)	-39.2 ± 4.5 ($n = 9$)	-40.1 ± 4.0 ($n = 5$)	-54.2 ± 2.5 ($n = 13$)	-58.9 ± 2.4 ($n = 16$)	-56.0 ± 2.4 ($n = 3$)	-70.2 ± 2.7 ($n = 8$)
$[Cl^-]_i$ (mM)	30.1 ± 1.9 ($n = 18$)	27.4 ± 4.4 ($n = 9$)	26.4 ± 3.8 ($n = 5$)	15.4 ± 1.4 ($n = 13$)	12.4 ± 1.1 ($n = 16$)	14.4 ± 1.3 ($n = 3$)	8.3 ± 0.8 ($n = 8$)

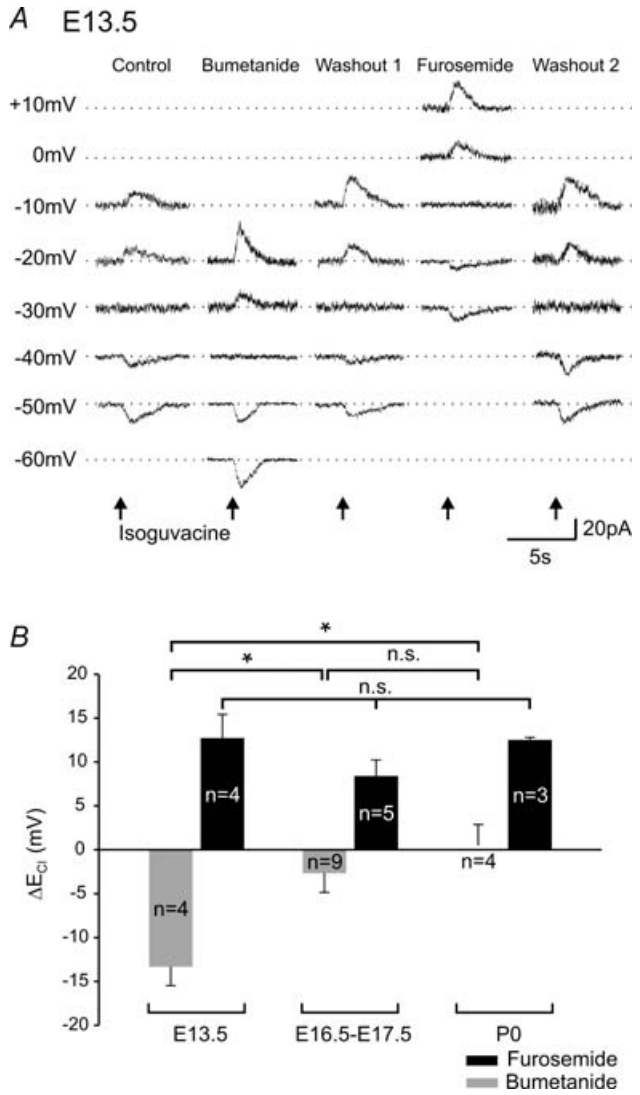

Figure 6. Functional role of KCC2 and NKCC1 at different stages of development

A, representative experiment at E13.5 illustrating the reversal of isoguvacine-evoked currents in control conditions, during the blockade of NKCC1 cotransporter (bumetanide, 20 μM, 40 min) or when the KCC2 cotransporter is blocked (furosemide, 200 μM, 5 min). All current traces are from the same E13.5 motoneuron. The duration of washout is around 30 min. *B,* quantitative analysis of the effects of the cotransporter blockers at three key developmental stages (E13.5, E16.5–E17.5 and P0). At E13.5, NKCC1 and KCC2 blockers induce opposite variations of E_{Cl}. At E16.5–E17.5, although KCC2 blocker remains efficient, blocking the NKCC1 cotransporter reveals a decreased effect on E_{Cl}. At P0, only the KCC2 blocker is effective. *n*, number of motoneurons tested; n.s., non-significant difference; * $P < 0.05$ (one-way ANOVA followed by a *post hoc* Tukey's test).

periods, i.e. E13.5, E16.5–E17.5 and P0. The reversal potential for $GABA_A$R-mediated current was determined, in voltage-clamp configuration, in control conditions and during bath application of either bumetanide (10–20 μM) or furosemide (50–200 μM). Bumetanide, a specific NKCC1 blocker at the concentration of 10–20 μM (Dzhala *et al.* 2005), was always applied first. Thus, opposite effects observed in the presence of furosemide, a less specific KCC2 blocker (Payne *et al.* 2003), could be attributed to KCC2 blockade. Figure 6*A* illustrates such an experimental protocol for E13.5 motoneurons. At this stage of development, application of bumetanide reversibly shifted the reversal for $GABA_A$R-mediated current to a more negative value (Fig. 6*A*, bumetanide and washout 1). By contrast, application of furosemide reversibly shifted E_{Cl} toward a more depolarized potential (Fig. 6*A*, furosemide and washout 2). Altogether these pharmacological experiments indicate that, at this early stage of development, both NKCC1 and KCC2 are functional on spinal motoneurons. We performed the same experiments at E16.5–E17.5 and P0, and quantified E_{Cl} variations at these stages (Fig. 6*B*). Whereas the blockade of KCC2 induced a depolarizing shift at all stages of embryonic development (Fig. 6*B*, black bars), NKCC1 blockade led to a hyperpolarizing shift at E13.5 that vanished after E16.5 (ΔE_{Cl} at E13.5 significantly different from ΔE_{Cl} at E16.5–E17.5 and P0, one-way ANOVA followed by Tukey's test) (Fig. 6*B*, grey bars). Under KCC2 blockade, the amplitude of the shift remained stable at all studied stages (12.7 ± 2.7 mV at E13.5, 7.1 ± 1.9 mV at E16.5–E17.5 and 12.5 ± 0.3 mV at P0) (no statistical difference, one-way ANOVA), indicating that this cotransporter remains functional during the whole course of embryonic development. By contrast, NKCC1 blockade induced an E_{Cl} shift of -13.5 ± 2.2 mV at E13.5 but failed to significantly modify E_{Cl} at later stages: the shift was -2.8 ± 2.3 mV at E16.5–E17.5 and 0.5 ± 2.4 mV at P0. Altogether, our data suggest that both chloride cotransporters are expressed concomitantly early in development but that they are sequentially functional: NKCC1 and KCC2 at early stages and then only KCC2.

Our macroscopic analysis shows that the mean level of both cotransporter proteins does not significantly change in the ventral area (Fig. 2). Because this mean level does not reflect the staining of any specific cell type (motoneurons, interneurons or glial cells), we analysed, at the cellular level, using a triple staining, the distribution of each

cotransporter in Neurobiotin-injected motoneurons. The distribution of NKCC1 and KCC2 proteins was analysed in the cytoplasm and in the vicinity of the plasma membrane of stained motoneurons. This work was performed at three specific stages: at E13.5 when E_{Cl} is at depolarized values, at E16.5 after the main drop of E_{Cl}, and at birth when E_{Cl} reaches V_{rest}. At E13.5, the injection of Neurobiotin revealed the morphological features of the motoneuron (Fig. 7*A*1) and indicated that numerous KCC2 clusters were present in the cytoplasm and in the vicinity of the neuronal plasma membrane (Fig. 7*A*2). This result was confirmed by the merged images of the KCC2 and Neurobiotin soma labelling using three-dimensional observations (Fig. 7*A*3–5, arrowheads). At P0, KCC2 labelling was also detected both in the cytoplasm and around the cell membrane (Fig. 7*B*2–5). Quantification of the KCC2 clusters in the cytoplasm indicated no changes between E13.5, E16.5 and P0 (Fig. 7*C*) (linear regression slope not significantly different from zero, $P = 0.8250$). On the contrary, clusters surrounding the motoneuronal membrane area decreased from E13.5 to P0 (Fig. 7*C*) (linear regression slope significantly different from zero, $P < 0.0001$). The NKCC1 labelling was also analysed in the cellular body of the same injected motoneurons. At E13.5, in addition to a dense labelling in the cytoplasm, NKCC1-ir clusters were detected at the level of the membrane (arrowheads, Fig. 7*A*6–9). At P0, the membrane and the cytoplasm still expressed NKCC1-ir (arrowheads, Fig. 7*B*6–9) but an apparent reduction of NKCC1 clusters was observed. Our quantitative analysis of the NKCC1 cluster density confirmed these observations: the NKCC1 cluster density decreased significantly from E13.5 to P0 in both the cytoplasm and the surrounding membrane area (linear regression slopes significantly different from zero, $P < 0.01$) (Fig. 7*D*).

Discussion

The results presented in this study show that (1) KCC2 and NKCC1 cotransporters are immunodetected in ventral areas at all embryonic stages from E11.5 to P0; (2) KCC2 and NKCC1 proteins are both functional at early stages (i.e. at E13.5); (3) KCC2 remains active from E13.5 until birth whereas NKCC1 becomes inefficient at E16.5 in spite of an immunohistochemical signature from E16.5 to P0; (4) E_{Cl} abruptly drops under spike threshold after E15.5. We can thus conclude that the NKCC1 inactivation during the fetal development of the mouse spinal cord alters the chloride equilibrium potential and therefore plays an important role in the maturation of $GABA_A$R-mediated inhibition in motor networks.

Ontogeny of KCC2 and NKCC1

Given the crucial contribution of the KCC2 and NKCC1 cotransporters to the maturation of inhibition in neural networks, many studies have been dedicated to the spatio-temporal analysis of their distribution in different CNS structures during development. However, it is difficult to draw consistent conclusions that could be applied to all CNS networks. In some structures, KCC2 protein level is low when networks are immature and then increases gradually towards its maximum in mature systems. Such is the case in the rodent cortex (Stein *et al.* 2004; Blaesse *et al.* 2006), the hippocampus (Lu *et al.* 1999; Gulyas *et al.* 2001; Stein *et al.* 2004), the inner plexiform layer of the turtle retina (Sernagor *et al.* 2003), the mouse retina (Zhang *et al.* 2007) and the mouse cerebellar granule cells (Takayama & Inoue, 2006). By contrast, the KCC2 immunoreactivity is comparable in immature and mature networks such as rat LSO (Blaesse *et al.* 2006) and cochlear nucleus (Vale *et al.* 2005). As described in these latter structures, our macroscopic results show a similar evolution of KCC2 in ventral areas of mouse spinal cord during fetal development. Interestingly, we find a similar amount of KCC2 protein in the motoneuronal cytoplasm at all embryonic stages studied.

Data from the literature indicate that the NKCC1 protein tends to decrease when the network matures. This is the case in cerebellar Purkinje cells after birth (Plotkin *et al.* 1997) and in the soma of CA3 pyramidal hippocampal cells even though labelling persists in the dendrites (Marty *et al.* 2002). At the macroscopic level, our data from embryonic mouse spinal cords reveal a constant level of NKCC1 staining in the ventral area from E11.5 to birth. However, when analysed at the specific motoneuronal level, NKCC1 protein level decreases during ontogeny both at the cytoplasm and soma membrane level. This discrepancy between the macroscopic constant level of NKCC1 and the microscopic reduction in stained motoneurons can be explained by a NKCC1 staining of other cellular populations (interneurons, glial cells) included in our macroscopic analysis.

From a functional point of view, our microscopic analysis of both cotransporters draws the three following remarks. First, the stable KCC2 density in the cytoplasm suggests a continuous protein synthesis and parallels the permanent functionality of this chloride extruder. Second, the decrease of NKCC1 activity is also in agreement with the reduction of the protein in the cytoplasm and in the cell membrane area. Third, given the NKCC1 inactivation, the lowering of KCC2 clusters at the plasma membrane may indicate that less KCC2 cotransporters are necessary to maintained low E_{Cl} values.

Development of inhibition in motoneurons: role of KCC2 and NKCC1

Studies performed in cortical and hippocampal networks have led to the accepted view that in immature networks GABA acts as an excitatory transmitter, whereas it switches

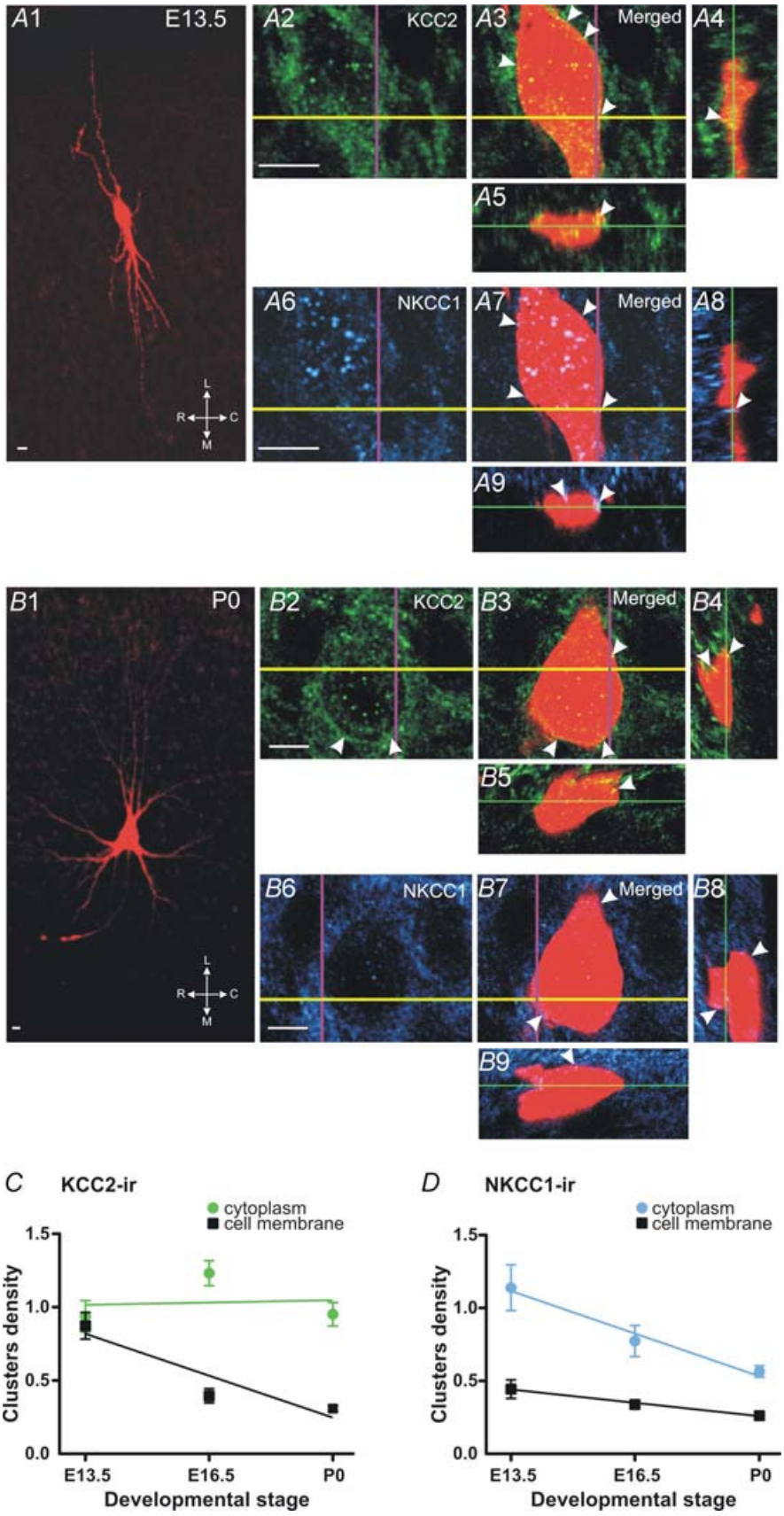

to an inhibitory transmitter when networks become mature. Cellular mechanisms by which this switch occurs have been extensively studied in these structures, and are thought to be based on the ontogenic decrease of the transmembrane chloride gradient, this decrease relying on the modification of the balance between the two chloride transporters KCC2 (Cl^- extruder) and NKCC1 (Cl^- uptake). The classical scheme proposes that, in immature neurons, NKCC1 is highly expressed compared to KCC2 and therefore $[Cl^-]_i$ is high, leading to excitatory GABAergic effects. In mature neurons, the cotransporter ratio is reversed leading to lower $[Cl^-]_i$ and inhibitory GABAergic effects (Ben-Ari, 2001, 2002; Owens & Kriegstein, 2002). This importance of KCC2 in the establishment of inhibition, first demonstrated in the hippocampus (Rivera *et al.* 1999), has recently been confirmed: it is indeed possible to induce a premature switch from GABA excitatory to inhibitory response by transfecting immature neurons with active KCC2 (Lee *et al.* 2005). However, while the functional role of KCC2 in the development of neuronal inhibition appears clear, the role of NKCC1 remains puzzling. For example, in the LSO, immature neurons (P3 stage of development) exhibiting excitatory glycinergic effects do not express NKCC1 mRNA. However, mature neurons (at P12), whose glycinergic effects have became inhibitory, surprisingly express NKCC1 mRNA (Balakrishnan *et al.* 2003). Also, in the mouse retina, NKCC1 does not mediate the accumulation of chloride in immature neurons (Zhang *et al.* 2007). By contrast, neocortical immature neurons (P1–P2) with depolarizing E_{GABA} express NKCC1 mRNA unlike more mature neurons (P11–P20) in which GABA inhibition has occurred because of a drop in E_{Cl} (Yamada *et al.* 2004). Similarly, in dorsal root ganglion neurons of homozygote NKCC1 null mice, E_{GABA} was significantly more negative, indicating that NKCC1 plays a major role in depolarizing GABA responses found in these mature neurons (Sung *et al.* 2000).

In mouse embryonic spinal cord, we have shown that the cotransporters KCC2 and NKCC1 are involved in the control of $[Cl^-]_i$ (Fig. 8). Whereas both cotransporters are expressed throughout embryonic development (Fig. 8*A*–*C*), the efficacy of NKCC1 and KCC2 evolved differentially: the chloride extruder KCC2 is active in immature and in behaviourally mature spinal networks while NKCC1 becomes inefficient during the maturation. Therefore, in the spinal cord, E_{Cl} maturation (i.e. $E_{GABA(A)R}$ and probably E_{GlyR}) may be explained by the NKCC1 inactivation.

The decrease of NKCC1 at the motoneuronal level suggests that its synthesis may remain at a low level at perinatal stages but may be reactivated under certain conditions, such as in the spinal dorsal horn after inflammatory insults or under chronic pain (Morales-Aza *et al.* 2004; Price *et al.* 2005). Two possibilities, not exclusive, may underlie NKCC1 reactivation. First, because the chloride uptake molecule NKCC1 may alternate between monomeric and oligomeric units (Simard *et al.* 2004), NKCC1 may be present as active oligomeric units in the immature lumbar spinal cord and become inactive as the subunits dissociate and become monomeric in mature tissue. Such developmentally regulated modifications have been recently described for KCC2, which becomes active after oligomerization in the LSO (Blaesse *et al.* 2006). Second, the NKCC1 protein may recover its efficacy by phosphorylation (Darman & Forbush, 2002) as described in the spinal cord where painful stimuli induced a rapid transient phosphorylation of NKCC1 probably involved in the initial generation of hyperalgesia (Galan & Cervero, 2005). Similarly, in hippocampal slices, ischaemia may also induce rapid increases of intracellular chloride concentration through NKCC1 phosphorylation (Pond *et al.* 2006).

Figure 7. Distribution of NKCC1 and KCC2 proteins on motoneurons
*A*1–9, confocal images of an E13.5 Neurobiotin-injected motoneuron (*A*1) show the presence of KCC2-ir (*A*2–5) and NKCC1-ir (*A*6–9) clusters in the cytoplasm and in the periphery of the cell membrane (arrowheads). *A*3 and *A*7 are image displays in *X*–*Y* direction. *A*4 and *A*8 are line images displayed in *X*–*Z* direction (at the level of the purple vertical line in *A*2–3, *A*6–7). *A*5 and *A*9 are line images displayed in *Y*–*Z* direction (at the level of the yellow horizontal line in *A*2–3, *A*6–7). *B*1–9, confocal views of a P0 Neurobiotin-injected motoneuron (*B*1). KCC2-ir clusters (*B*2–5) appear dense in the cytoplasm and in the periphery of the cell membrane (arrowheads) while NKCC1-ir clusters, although still detected close to the cell membrane (arrowheads), appear less numerous in the cytoplasm (*B*6–9). Same multi-plane views as in *A*. Images are single optical sections (0.2 μm thick). *C* and *D*, quantitative analysis of the density (number per volume in μm^3) of KCC2- and NKCC1-ir clusters in the cytoplasm and in the vicinity of the plasma membrane. KCC2-ir cluster density appears stable in the cytoplasm during the entire embryonic life (green circles) and decreases in the vicinity of cell membrane (black squares). NKCC1 cluster density diminishes during development in the cytoplasm (blue circles) and around the plasma membrane (black squares). Linear regression analysis for KCC2-ir clusters: slope significantly different from zero in the cytoplasm ($P < 0.0001$) but not around the cell membrane ($P = 0.8250$). Linear regression analysis for NKCC1 clusters: slope significantly non-zero in the cytoplasm ($P < 0.01$) and around the cell membrane ($P < 0.01$). Scale bars, 10 μm. C, caudal; L, lateral; M, medial; R, rostral. Data, from 5–6 Neurobiotin-injected motoneurons at each stage, are expressed as means ± S.E.M.

Ontogenetic evolution of intracellular chloride concentration

The $GABA_AR$ equilibrium potential is commonly monitored to calculate the $[Cl^-]_i$. A progressive decrease of $[Cl^-]_i$ during the course of development has been suggested by comparing two key stages (Owens *et al.* 1996; Ehrlich *et al.* 1999; Ritter & Zhang, 2000; Balakrishnan *et al.* 2003). In the present study, we give rise to a different view: instead of a linear decrease of E_{Cl}, lumbar spinal motoneurons exhibit a dramatic drop of E_{Cl} between E15.5 and E16.5 (Fig. 5). Remarkably, this abrupt change is concomitant with other important changes during the behavioural maturation of the embryonic mouse spinal motoneuronal network. First, at E15.5, motoneuronal membrane input resistances reach more mature values (see Fig. 3*D*). Second, at E14.5 (one day before this drop) 5-HT descending inputs reach lumbar levels (Ballion *et al.* 2002) controlling the GABA phenotype expression (Allain *et al.* 2005) and the expression of inhibition (Branchereau *et al.* 2002). Third, again at E14.5, the mouse spinal cord shows a peak of spontaneous activity followed at E15.5 by a silent period (Yvert *et al.* 2004). Fourth, at around E17.5 fictive alternate locomotor activity may be elicited by 5-HT bath application (Branchereau *et al.* 2000). Interestingly, whereas at E17.5 the lumbar spinal networks may express a left–right coordination suggesting the presence of inhibitions between ipsi- and contralateral sides, the mouse spinal motoneurons still exhibit depolarizing E_{Cl} after the E16.5 stage (see Figs 4 and 5*C*). Such inhibitions between ipsi- and contralateral sides may be rendered possible if we consider that, at E16.5, GABA/glycine inputs exert shunting effects due to the presence of E_{Cl} above the resting membrane potential but largely below the spike threshold (Fig. 5). Shunting effects of depolarizing GABA/glycine have already been described in cortex (Gulledge & Stuart, 2003).

In the present study, using immunocytochemistry and perforated patch clamp combined with pharmacology, we identified a precise landmark (E16.5) in the development of the embryonic spinal cord during which the very first inhibition can occur. Such early inhibition can be explained by an abrupt drop of $[Cl^-]_i$ due to NKCC1 inactivation. Why is it important to clearly identify the embryonic maturation of inhibition within the spinal motoneuron? To date, most studies investigating the maturation of locomotor central pattern generators (CPGs) in parallel with the evolution of the GABA/glycine system have been based on perinatal analysis of motoneuronal outputs in wild-type and/or genetically modified animals (Kullander *et al.* 2003; Kiehn & Kullander, 2004; Lanuza *et al.* 2004; Hinckley *et al.* 2005; Gosgnach *et al.* 2006). However, while these studies may illuminate the role of specific neuronal categories in the final organization of the motor networks, they do not really shed light on how such CPG networks emerge during embryonic life and interact with motoneurons. We believe our observations on the maturation of motoneuronal properties and their inhibitory interactions with GABA/glycine interneurons will be very useful to understand (1) emergence of alternating patterns between mature motoneuronal pools, and (2) construction of rhythm generator networks that probably include motoneuronal populations (Mentis *et al.* 2005). Finally, our data may be crucial to explore new approaches to functional recovery of injured spinal motoneurons because these neurons regain embryonic-like properties (Jean-Xavier *et al.* 2006).

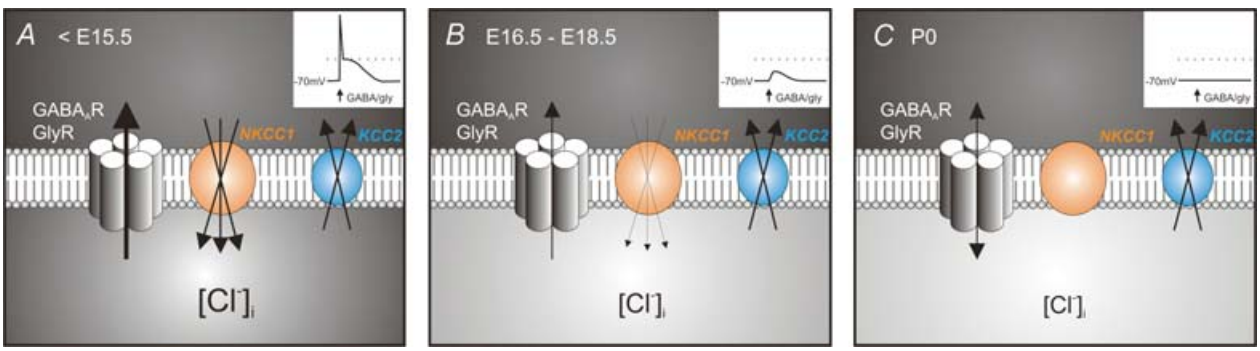

Figure 8. Mechanisms underlying the developmental shift in $GABA_AR$/GlyR responses in the mouse spinal cord
A, before E15.5, both KCC2 and NKCC1 are active and $[Cl^-]_i$ is high. Therefore, the activation of the Cl^--gated receptors induces a large outward chloride current that depolarizes the membrane and triggers action potentials (see inset, right upper corner). *B,* between E16.5 and E18.5, $[Cl^-]_i$ is reduced due to a decrease of the NKCC1 efficacy. At these stages, although the activation of $GABA_AR$ and GlyR leads to depolarization, no action potential is elicited (inset). *C,* at birth, NKCC1 has lost its efficiency and only the chloride extruder KCC2 remains functional, lowering $[Cl^-]_i$. Inset: around resting potential, the activation of $GABA_AR$/GlyR does not modify the membrane potential.

Knowledge of the mechanisms underlying the maturation of motoneurons will undoubtedly help to recapitulate the ontogenic maturation of these traumatized cells.

References

Allain AE, Bairi A, Meyrand P & Branchereau P (2004). Ontogenic changes of the GABAergic system in the embryonic mouse spinal cord. *Brain Res* **1000**, 134–147.

Allain AE, Bairi A, Meyrand P & Branchereau P (2006). Expression of the glycinergic system during the course of embryonic development in the mouse spinal cord and its co-localization with GABA immunoreactivity. *J Comp Neurol* **496**, 832–846.

Allain AE, Meyrand P & Branchereau P (2005). Ontogenic changes of the spinal GABAergic cell population are controlled by the serotonin (5-HT) system: implication of 5-HT1 receptor family. *J Neurosci* **25**, 8714–8724.

Alvarez-Leefmans FJ, Gamino SM, Giraldez F & Nogueron I (1988). Intracellular chloride regulation in amphibian dorsal root ganglion neurones studied with ion-selective microelectrodes. *J Physiol* **406**, 225–246.

Baccei ML & Fitzgerald M (2004). Development of GABAergic and glycinergic transmission in the neonatal rat dorsal horn. *J Neurosci* **24**, 4749–4757.

Balakrishnan V, Becker M, Lohrke S, Nothwang HG, Guresir E & Friauf E (2003). Expression and function of chloride transporters during development of inhibitory neurotransmission in the auditory brainstem. *J Neurosci* **23**, 4134–4145.

Ballion B, Branchereau P, Chapron J & Viala D (2002). Ontogeny of descending serotonergic innervation and evidence for intraspinal 5-HT neurons in the mouse spinal cord. *Dev Brain Res* **137**, 81–88.

Banke TG & McBain CJ (2006). GABAergic input onto CA3 hippocampal interneurons remains shunting throughout development. *J Neurosci* **26**, 11720–11725.

Ben-Ari Y (2001). Developing networks play a similar melody. *Trends Neurosci* **24**, 353–360.

Ben-Ari Y (2002). Excitatory actions of GABA during development: the nature of the nurture. *Nat Rev Neurosci* **3**, 728–739.

Ben-Ari Y, Cherubini E, Corradetti R & Gaiarsa JL (1989). Giant synaptic potentials in immature rat CA3 hippocampal neurones. *J Physiol* **416**, 303–325.

Blaesse P, Guillemin I, Schindler J, Schweizer M, Delpire E, Khiroug L, Friauf E & Nothwang HG (2006). Oligomerization of KCC2 correlates with development of inhibitory neurotransmission. *J Neurosci* **26**, 10407–10419.

Branchereau P, Chapron J & Meyrand P (2002). Descending 5-hydroxytryptamine raphe inputs repress the expression of serotonergic neurons and slow the maturation of inhibitory systems in mouse embryonic spinal cord. *J Neurosci* **22**, 2598–2606.

Branchereau P, Morin D, Bonnot A, Ballion B, Chapron J & Viala D (2000). Development of lumbar rhythmic networks: from embryonic to neonate locomotor-like patterns in the mouse. *Brain Res Bull* **53**, 711–718.

Clarac F, Brocard F & Vinay L (2004). The maturation of locomotor networks. *Prog Brain Res* **143**, 57–66.

Cordero-Erausquin M, Coull JA, Boudreau D, Rolland M & De Koninck Y (2005). Differential maturation of GABA action and anion reversal potential in spinal lamina I neurons: impact of chloride extrusion capacity. *J Neurosci* **25**, 9613–9623.

Darman RB & Forbush B (2002). A regulatory locus of phosphorylation in the N terminus of the Na-K-Cl cotransporter, NKCC1. *J Biol Chem* **277**, 37542–37550.

Delpy A, Allain A-E, Meyrand P & Branchereau P (2006). Ontogeny of NKCC1 and KCC2 in parallel with the maturation of inhibition within the embryonic mouse spinal cord. *Abstr Soc Neurosci* 716.11.

Dzhala VI, Talos DM, Sdrulla DA, Brumback AC, Mathews GC, Benke TA, Delpire E, Jensen FE & Staley KJ (2005). NKCC1 transporter facilitates seizures in the developing brain. *Nat Med* **11**, 1205–1213.

Ehrlich I, Lohrke S & Friauf E (1999). Shift from depolarizing to hyperpolarizing glycine action in rat auditory neurones is due to age-dependent Cl^- regulation. *J Physiol* **520**, 121–137.

Galan A & Cervero F (2005). Painful stimuli induce *in vivo* phosphorylation and membrane mobilization of mouse spinal cord NKCC1 co-transporter. *Neuroscience* **133**, 245–252.

Gao BX, Cheng G & Ziskind-Conhaim L (1998). Development of spontaneous synaptic transmission in the rat spinal cord. *J Neurophysiol* **79**, 2277–2287.

Gao BX, Stricker C & Ziskind-Conhaim L (2001). Transition from GABAergic to glycinergic synaptic transmission in newly formed spinal networks. *J Neurophysiol* **86**, 492–502.

Gosgnach S, Lanuza GM, Butt SJ, Saueressig H, Zhang Y, Velasquez T, Riethmacher D, Callaway EM, Kiehn O & Goulding M (2006). V1 spinal neurons regulate the speed of vertebrate locomotor outputs. *Nature* **440**, 215–219.

Grillner S & Wallen P (1985). Central pattern generators for locomotion, with special reference to vertebrates. *Annu Rev Neurosci* **18**, 233–261.

Gulledge AT & Stuart GJ (2003). Excitatory actions of GABA in the cortex. *Neuron* **37**, 299–309.

Gulyas AI, Sik A, Payne JA, Kaila K & Freund TF (2001). The KCl cotransporter, KCC2, is highly expressed in the vicinity of excitatory synapses in the rat hippocampus. *Eur J Neurosci* **13**, 2205–2217.

Hinckley C, Seebach B & Ziskind-Conhaim L (2005). Distinct roles of glycinergic and GABAergic inhibition in coordinating locomotor-like rhythms in the neonatal mouse spinal cord. *Neuroscience* **131**, 745–758.

Hubner CA, Stein V, Hermans-Borgmeyer I, Meyer T, Ballanyi K & Jentsch TJ (2001). Disruption of KCC2 reveals an essential role of K-Cl cotransport already in early synaptic inhibition. *Neuron* **30**, 515–524.

Jean-Xavier C, Pflieger JF, Liabeuf S & Vinay L (2006). Inhibitory postsynaptic potentials in lumbar motoneurons remain depolarizing after neonatal spinal cord transection in the rat. *J Neurophysiol* **96**, 2274–2281.

Khazipov R, Khalilov I, Tyzio R, Morozova E, Ben-Ari Y & Holmes GL (2004). Developmental changes in GABAergic actions and seizure susceptibility in the rat hippocampus. *Eur J Neurosci* **19**, 590–600.

Kiehn O (2006). Locomotor circuits in the mammalian spinal cord. *Annu Rev Neurosci* **29**, 279–306.

Kiehn O & Butt SJ (2003). Physiological, anatomical and genetic identification of CPG neurons in the developing mammalian spinal cord. *Prog Neurobiol* **70**, 347–361.

Kiehn O & Kullander K (2004). Central pattern generators deciphered by molecular genetics. *Neuron* **41**, 317–321.

Kudo N & Nishimaru H (1998). Reorganization of locomotor activity during development in the prenatal rat. *Ann N Y Acad Sci* **860**, 306–317.

Kullander K, Butt SJ, Lebret JM, Lundfald L, Restrepo CE, Rydstrom A, Klein R & Kiehn O (2003). Role of EphA4 and EphrinB3 in local neuronal circuits that control walking. *Science* **299**, 1889–1892.

Lanuza GM, Gosgnach S, Pierani A, Jessell TM & Goulding M (2004). Genetic identification of spinal interneurons that coordinate left-right locomotor activity necessary for walking movements. *Neuron* **42**, 375–386.

Lee H, Chen CX, Liu YJ, Aizenman E & Kandler K (2005). KCC2 expression in immature rat cortical neurons is sufficient to switch the polarity of GABA responses. *Eur J Neurosci* **21**, 2593–2599.

Lu J, Karadsheh M & Delpire E (1999). Developmental regulation of the neuronal-specific isoform of K-Cl cotransporter KCC2 in postnatal rat brains. *J Neurobiol* **39**, 558–568.

Marty S, Wehrle R, Alvarez-Leefmans FJ, Gasnier B & Sotelo C (2002). Postnatal maturation of Na^+, K^+, $2Cl^-$ cotransporter expression and inhibitory synaptogenesis in the rat hippocampus: an immunocytochemical analysis. *Eur J Neurosci* **15**, 233–245.

Mentis GZ, Alvarez FJ, Bonnot A, Richards DS, Gonzalez-Forero D, Zerda R & O'Donovan MJ (2005). Noncholinergic excitatory actions of motoneurons in the neonatal mammalian spinal cord. *Proc Natl Acad Sci U S A* **102**, 7344–7349.

Morales-Aza BM, Chillingworth NL, Payne JA & Donaldson LF (2004). Inflammation alters cation chloride cotransporter expression in sensory neurons. *Neurobiol Dis* **17**, 62–69.

Owens DF, Boyce LH, Davis MB & Kriegstein AR (1996). Excitatory GABA responses in embryonic and neonatal cortical slices demonstrated by gramicidin perforated-patch recordings and calcium imaging. *J Neurosci* **16**, 6414–6423.

Owens DF & Kriegstein AR (2002). Is there more to GABA than synaptic inhibition? *Nat Rev Neurosci* **3**, 715–727.

Payne JA, Rivera C, Voipio J & Kaila K (2003). Cation-chloride co-transporters in neuronal communication, development and trauma. *Trends Neurosci* **26**, 199–206.

Payne JA, Stevenson TJ & Donaldson LF (1996). Molecular characterization of a putative K-Cl cotransporter in rat brain. A neuronal-specific isoform. *J Biol Chem* **271**, 16245–16252.

Plotkin MD, Snyder EY, Hebert SC & Delpire E (1997). Expression of the Na-K-2Cl cotransporter is developmentally regulated in postnatal rat brains: a possible mechanism underlying GABA's excitatory role in immature brain. *J Neurobiol* **33**, 781–795.

Pond BB, Berglund K, Kuner T, Feng G, Augustine GJ & Schwartz-Bloom RD (2006). The chloride transporter Na^+-K^+-Cl^- cotransporter isoform-1 contributes to intracellular chloride increases after *in vitro* ischemia. *J Neurosci* **26**, 1396–1406.

Price TJ, Cervero F & de Koninck Y (2005). Role of cation-chloride-cotransporters (CCC) in pain and hyperalgesia. *Curr Top Med Chem* **5**, 547–555.

Quinlan KA & Kiehn O (2007). Segmental, synaptic actions of commissural interneurons in the mouse spinal cord. *J Neurosci* **27**, 6521–6530.

Ritter B & Zhang W (2000). Early postnatal maturation of $GABA_A$-mediated inhibition in the brainstem respiratory rhythm-generating network of the mouse. *Eur J Neurosci* **12**, 2975–2984.

Rivera C, Voipio J, Payne JA, Ruusuvuori E, Lahtinen H, Lamsa K, Pirvola U, Saarma M & Kaila K (1999). The K^+/Cl^- co-transporter KCC2 renders GABA hyperpolarizing during neuronal maturation. *Nature* **397**, 251–255.

Rohrbough J & Spitzer NC (1996). Regulation of intracellular Cl^- levels by Na^+-dependent Cl^- cotransport distinguishes depolarizing from hyperpolarizing $GABA_A$ receptor-mediated responses in spinal neurons. *J Neurosci* **16**, 82–91.

Russell JM (2000). Sodium-potassium-chloride cotransport. *Physiol Rev* **80**, 211–276.

Sernagor E, Young C & Eglen SJ (2003). Developmental modulation of retinal wave dynamics: shedding light on the GABA saga. *J Neurosci* **23**, 7621–7629.

Simard CF, Brunet GM, Daigle ND, Montminy V, Caron L & Isenring P (2004). Self-interacting domains in the C terminus of a cation-Cl^- cotransporter described for the first time. *J Biol Chem* **279**, 40769–40777.

Singer JH, Talley EM, Bayliss DA & Berger AJ (1998). Development of glycinergic synaptic transmission to rat brain stem motoneurons. *J Neurophysiol* **80**, 2608–2620.

Stein V, Hermans-Borgmeyer I, Jentsch TJ & Hubner CA (2004). Expression of the KCl cotransporter KCC2 parallels neuronal maturation and the emergence of low intracellular chloride. *J Comp Neurol* **468**, 57–64.

Sung KW, Kirby M, McDonald MP, Lovinger DM & Delpire E (2000). Abnormal $GABA_A$ receptor-mediated currents in dorsal root ganglion neurons isolated from Na-K-2Cl cotransporter null mice. *J Neurosci* **20**, 7531–7538.

Takayama C & Inoue Y (2006). Developmental localization of potassium chloride co-transporter 2 in granule cells of the early postnatal mouse cerebellum with special reference to the synapse formation. *Neuroscience* **143**, 757–767.

Tyzio R, Ivanov A, Bernard C, Holmes GL, Ben-Ari Y & Khazipov R (2003). Membrane potential of CA3 hippocampal pyramidal cells during postnatal development. *J Neurophysiol* **90**, 2964–2972.

Vale C, Caminos E, Martinez-Galan JR & Juiz JM (2005). Expression and developmental regulation of the K^+-Cl^- cotransporter KCC2 in the cochlear nucleus. *Hear Res* **206**, 107–115.

Vinay L, Brocard F, Pflieger JF, Simeoni-Alias J & Clarac F (2000). Perinatal development of lumbar motoneurons and their inputs in the rat. *Brain Res Bull* **53**, 635–647.

Wu WL, Ziskind-Conhaim L & Sweet MA (1992). Early development of glycine- and GABA-mediated synapses in rat spinal cord. *J Neurosci* **12**, 3935–3945.

Yamada J, Okabe A, Toyoda H, Kilb W, Luhmann HJ & Fukuda A (2004). Cl^- uptake promoting depolarizing GABA actions in immature rat neocortical neurones is mediated by NKCC1. *J Physiol* **557**, 829–841.

Yvert B, Branchereau P & Meyrand P (2004). Multiple spontaneous rhythmic activity patterns generated by the embryonic mouse spinal cord occur within a specific developmental time window. *J Neurophysiol* **91**, 2101–2109.

Zhang LL, Delpire E & Vardi N (2007). NKCC1 does not accumulate chloride in developing retinal neurons. *J Neurophysiol* **98**, 266–277.

Acknowledgements

The authors thank Drs J. Golowasch and B. Yvert for critical readings of the manuscript. They also thank Philippe Chauvet for technical support. This study was supported by grants from the Conseil Régional d'Aquitaine (no. 20040301202A) and the Institut pour la Recherche sur la Moelle épinière et l'Encéphale (IRME/2005/2006).